photonics

MDPI

Article

A Compact and Robust Polarization-Entangled Photon Source Towards Application in Mobile Platforms

Jing Wang †, Peng Li †, Luyi Sun, Pengcheng Wang, Nachuan Li, Xiao-Tian Zhang, Yan-Xiao Gong, Hua-Ying Liu *, Shi-Ning Zhu and Zhenda Xie

National Laboratory of Solid State Microstructures, School of Electronic Science and Engineering, School of Physics, College of Engineering and Applied Sciences, Collaborative Innovation Center of Advanced Microstructures, Nanjing University, Nanjing 210093, China; 602024220075@smail.nju.edu.cn (J.W.); 201870015@smail.nju.edu.cn (P.L.); 652023220042@smail.nju.edu.cn (L.S.); 602023220066@smail.nju.edu.cn (P.W.); 602024220039@smail.nju.edu.cn (N.L.); mg21220194@smail.nju.edu.cn (X.-T.Z.); gongyanxiao@nju.edu.cn (Y.-X.G.); zhusn@nju.edu.cn (S.-N.Z.); xiezhenda@nju.edu.cn (Z.X.)

* Correspondence: liuhuaying@nju.edu.cn

† These authors contributed equally to this work.

Abstract

Entangled-photon sources are indispensable components in free-space quantum key distribution (QKD) systems. Here, we present a compact, lightweight, and robust airborne entangled-photon source (AEPS) based on a Sagnac loop structure with single-mode fiber coupling. To meet the drone requirements for miniaturization, lightweight design, and high robustness, we developed a highly integrated entangled-photon source using customized miniature optical components and an adhesive bonding technique. The total volume and weight are only 38 × 40 × 24 mm^3 and 58 g, respectively. Entangled-photon pairs at 810 nm are generated via Type-II spontaneous parametric down-conversion (SPDC) in a periodically poled $KTiOPO_4$ (PPKTP) crystal. We achieve a quantum state fidelity of $F = 0.986 \pm 0.0017$, a photon-pair generation rate of 3.03×10^6 pairs/s/mW, and a CHSH Bell parameter of $S = 2.764 \pm 0.082$. Owing to its excellent size, weight, performance, and stability, the proposed entangled-photon source is particularly well suited for drone-based free-space mobile quantum communication.

Keywords: compact entangled-photon source; SPDC; Sagnac loop; QKD; PPKTP; drone; mobile quantum network

1. Introduction

Quantum entangled-photon sources are essential components in numerous systems, such as quantum communication [1–4], quantum computing [5,6], quantum precision measurement [7,8], and quantum imaging [9,10]. Photons encoded in the polarization degree of freedom are commonly employed for QKD and entanglement distribution in free space. According to the quantum no-cloning theorem and Heisenberg's uncertainty principle, quantum communication offers theoretically unbreakable security, meeting the growing demand for secure communication. This has made it a major research focus in the field of communication. Various mobile platforms have been explored for free-space demonstrations of entanglement distribution and QKD, including satellite-to-ground [4,11,12], drone-to-drone [3,13], drone-to-ground [1–3,14], drone-to-vehicle [13,14], and vehicle-to-vehicle [14,15] links. Compared with other free-space links, drones, as a novel quantum communication platform, offer high mobility, low cost, and flexible deployment, making

Check for updates

Received: 18 January 2026
Revised: 5 February 2026
Accepted: 10 February 2026
Published: 13 February 2026

Copyright: © 2026 by the authors. Licensee MDPI, Basel, Switzerland. This article is an open access article distributed under the terms and conditions of the Creative Commons Attribution (CC BY) license.

them an ideal platform for constructing low-altitude mobile quantum networks and a valuable complement to satellite-to-ground links [2,3].

However, the drone platform imposes strict limitations on weight, volume, and power consumption, requiring the quantum system to be as compact and lightweight as possible. This is crucial for enhancing the drone's flight endurance and enabling flexible deployment. To meet the requirements of satellite-based quantum communication, the Micius quantum science satellite developed and deployed the first spaceborne entangled-photon source capable of stable on-orbit operation [11]. Liu et al. built AEPS with Sagnac interference of two-sided pumped Type-II SPDC to achieve the first mobile entanglement distribution based on drones [2]. In addition, Omshankar et al. implemented a high-brightness polarization-entangled photon-pair source at 800 nm via SPDC in a 3 cm long Type-II PPKTP crystal pumped unidirectionally in a single-pass geometry [16]. These entangled-photon sources based on bulk optical components tend to have large volume and weight, making them unsuitable for integration onto drones. Therefore, the development of a compact, lightweight, and robust entangled-photon source for drone platforms holds significant practical value for establishing quantum communication links on mobile platforms.

Regarding the integration of entangled-photon sources, numerous efforts have been made to develop various on-chip entangled-photon sources. These sources typically utilize the SPDC process in periodically poled second-order nonlinear materials, such as lithium niobate [17,18], gallium arsenide [19], and aluminum nitride [20], or the four-wave mixing (FWM) process in third-order nonlinear materials, such as silicon carbide (SiC) [21,22] and silicon-based materials [23], to generate entangled-photon pairs. On-chip entangled sources offer advantages of compactness and integration, and most exhibit high spectral brightness. However, the entangled photons generated by these sources are usually in the communication band around 1550 nm, where the quantum efficiency of commonly used silicon avalanche photodiodes (Si-APDs) is extremely low. As a result, superconducting nanowire single-photon detectors (SNSPDs) are typically employed to detect the single photons. However, SNSPDs are bulky and power-hungry, making them unsuitable for integration onto mobile platforms such as drones and satellites.

To this end, we propose a compact entangled-photon source built using miniature bulk optics and adhesive bonding techniques. This source achieves high integration and lightweight design while maintaining performance comparable to traditional entangled-photon sources. The proposed source utilizes a Type-II SPDC process in a PPKTP crystal to generate pairs of polarization-entangled photons. We have implemented a fiber-coupled Sagnac loop structure on a silicon substrate to create the entangled-photon source. The dimensions of our source are only $38 \times 40 \times 24$ mm^3, with a weight of just 58 g, representing a size and weight reduction by approximately one to two orders of magnitude compared to traditional bulk-optics-based entangled sources. The experimentally measured Bell parameter is 2.764 ± 0.082, approaching the Bell inequality limit, while the fidelity obtained from quantum state tomography is 0.986 ± 0.0017. The entanglement visibility at the $|H\rangle$, $|V\rangle$, $|D\rangle$, and $|A\rangle$ bases are 98.6%, 98.7%, 96.7%, and 97.9%, respectively. The photon-pair generation rate is 3.03×10^6 pairs/s/mW. A performance comparison between our work and previously reported entangled-photon sources of the same type is shown in Table 1. Our results demonstrate that, despite its compact size and low weight, the performance of our entangled-photon source is comparable to that of bulk-optics-based sources, making it particularly suitable for entanglement distribution experiments on mobile platforms such as small drones. This work has the potential to accelerate the development of future mobile quantum networks.

Table 1. Comparison of this work with previously reported compact Sagnac-based polarization-entangled photon sources.

	Type	Size	Weight	Generation Rate * (Pairs/s/mW)	Fidelity	S-Parameter
This work	Type-II PPKTP crystal	38 mm × 40 mm × 24 mm	58 g	3.03×10^6	0.986	2.764
Yin (2017) [11]	Type-II PPKTP crystal	430 mm × 350 mm × 150 mm	23.8 kg	1.97×10^5	0.907	2.37
Liu (2020) [2]	Type-II PPKTP crystal	-	468 g	1.6×10^5	-	2.725
Omshankar (2024) [16]	Type-II PPKTP crystal	-	-	2.36×10^5	>0.95	2.68

* The generation rate reported here refers to the generated photon-pair rate inside the nonlinear crystal.

2. Materials and Methods

2.1. Experimental Principle

Various methods have been developed to generate entangled-photon pairs, with common techniques including the SPDC process in nonlinear optics [1,2,24], spontaneous four-wave mixing [21,25], quantum dots [26], and more. Recently, some researchers have proposed methods based on metasurfaces to generate entangled-photon pairs [27,28]. Each of these methods has its advantages and disadvantages, and the SPDC-based entangled-photon source is widely used due to its high brightness, simple structure, and mature technology.

This experiment employs Type-II SPDC, in which the generated photon pairs have orthogonal polarization, i.e., o(e) → o(e) + e(o), where "o" represents ordinary light and "e" represents extraordinary light, with their polarizations being perpendicular to each other. For the case of the collinear and degenerate Type-II SPDC, which is the focus of this work, phase matching requires momentum conservation among the pump and down-converted photons within the nonlinear crystal.

Under the phase-matching condition, the refractive indices of the pump and the down-converted photons inside the nonlinear crystal are required to be equal. However, in practice, nonlinear crystals exhibit dispersion effects, resulting in different phase velocities for the pump and down-converted photons. As a result, after propagating a certain distance through the crystal, a wavevector mismatch $\Delta \boldsymbol{k}$ occurs. This phase mismatch prevents coherent buildup of the SPDC amplitudes along the crystal length, leading to destructive interference and a significant reduction in the down-conversion efficiency.

To eliminate the dispersion effects in the crystal and satisfy the phase-matching condition in the SPDC process, quasi-phase matching (QPM) was proposed by Bloembergen et al. [29] in 1962. The core idea is to artificially create a periodic structure that provides an additional wavevector (i.e., reciprocal lattice vector G_m) to compensate for the wavevector mismatch Δk caused by dispersion. Entangled-photon sources based on QPM-enhanced SPDC allow for collinear propagation of the pump and down-converted photons, eliminating the walk-off effect. This enables the use of longer crystals, which increases the photon-pair generation rate and spectral brightness.

There are several methods for generating polarization-entangled photon pairs using the SPDC process, including post-selection, cross-crystal, dual-periodic crystal, beam-like, folded sandwich, Mach–Zehnder interferometer, and Sagnac interferometer approaches. Each method has its advantages and disadvantages, with a detailed discussion of these schemes found in the literature [30]. In this work, we selected the single-crystal Sagnac loop structure to generate pairs of polarization-entangled photons. Compared to other methods, the common-path design of the Sagnac loop makes it insensitive to environmental temperature fluctuations and mechanical vibrations, thus providing excellent phase stability. Additionally, it offers high generation efficiency. Considering the operational environment of our AEPS, we chose the Sagnac ring structure for building the entangled-photon source.

The length of the PPKTP crystal in the Sagnac loop is 20 mm, with a polarization period Λ of 10.025 μm.

2.2. Experimental Setup

Figure 1a shows the schematic of the fiber-coupled Sagnac-type polarization-entangled photon source. A self-injection-locked 405 nm continuous-wave diode laser (CP-405-PLR40, Ondex, Monrovia, CA, USA) is employed as the pump source. The laser exhibits a central wavelength of 405 nm with a thermal wavelength stability of 0.015 nm/°C and a linewidth of approximately 160 MHz after self-injection locking. A polarization extinction ratio of about 100:1 is achieved, which is sufficient for stable polarization-entangled photon-pair generation in our work. The general operation of the source is as follows: the pump source is focused by a lens and then split by a polarization beam splitter into V- and H-polarized components, which propagate through the PPKTP crystal in clockwise and counterclockwise directions, respectively. The V-polarized beam interacts with the PPKTP crystal via a dual-wavelength half-wave plate (D-HWP), generating a Type-II SPDC process and producing an 810 nm polarization-orthogonal photon pair $|H\rangle_s|V\rangle_i$, where $|H\rangle$ and $|V\rangle$ denote the horizontal and vertical polarization states of the photons, and the subscripts s and i represent the signal and idler photons. Similarly, the H-polarized beam generates a Type-II SPDC pair $|H\rangle_s|V\rangle_i$ in the crystal, which is converted to $|V\rangle_s|H\rangle_i$ after passing through the D-HWP. Finally, the clockwise and counterclockwise photon pairs interfere at PBS 1, producing the two-photon state $\left(|H\rangle_s|V\rangle_i + e^{i\phi}|V\rangle_s|H\rangle_i\right)/\sqrt{2}$. By adjusting QWP 1 and HWP 1, the relative phase ϕ can be controlled to obtain the Bell state $(|H\rangle_s|V\rangle_i - |V\rangle_s|H\rangle_i)/\sqrt{2}$.

Figure 1b,c shows the measurement setups used to characterize the biphoton entangled states. When only a half-wave plate is included in the optical path, the measurement setups can be used to test the CHSH inequality and entanglement correlation curves. When a quarter-wave plate is added to the measurement setups, it enables quantum state tomography. Details regarding the CHSH inequality and quantum state tomography are discussed in Section 3.

Traditional entangled-photon sources based on bulk-optics components typically use optomechanical elements such as mirror mounts and clamping forks to secure optical components on a breadboard. Therefore, the long-term stability of the entangled source performance depends on the structural stability of these optomechanical components. However, over time and with environmental changes (e.g., vibrations of the optical platform), small changes in the angles and positions of the mirror mounts can occur, ultimately leading to a deterioration in the performance of the entangled source. Beckert et al. [31] have demonstrated that the instability of the mounting components in the optical path is a major cause of the degradation in entangled source performance.

The payload capacity of a drone is strictly limited, making the development of a highly integrated entangled-photon source essential for drone-based mobile quantum communication. To achieve compactness and robustness, we replaced conventional bulky and unstable optomechanical components with an adhesive assembly technique, in which all optical elements were directly bonded onto a polished monocrystalline silicon substrate. The source employs miniaturized bulk optical components that were custom-designed according to the optical layout and beam size. Both the PPKTP crystal and the micro-optics were anti-reflection coated to reduce pump and photon-pair losses, thereby improving brightness.

To satisfy the QPM condition and achieve maximum down-conversion efficiency in the PPKTP crystal, a thermoelectric cooler (TEC) was placed beneath the silicon substrate to stabilize the crystal temperature at 23.5 °C. In addition, since our entanglement source is nearly coin-sized, a single TEC is sufficient to maintain the entire source at 23.5 °C, thereby

suppressing environmental temperature fluctuations and ensuring superior thermal stability. The optical components were fixed using ultraviolet-curable adhesive (NOA61, Norland Products Incorporated, Jamesburg, NJ, USA), which features an extremely low coefficient of thermal expansion (1–14 ppm/°C) and high bonding strength. With proper UV curing procedures, the miniature optical elements can be firmly attached to the silicon baseplate while maintaining long-term performance stability.

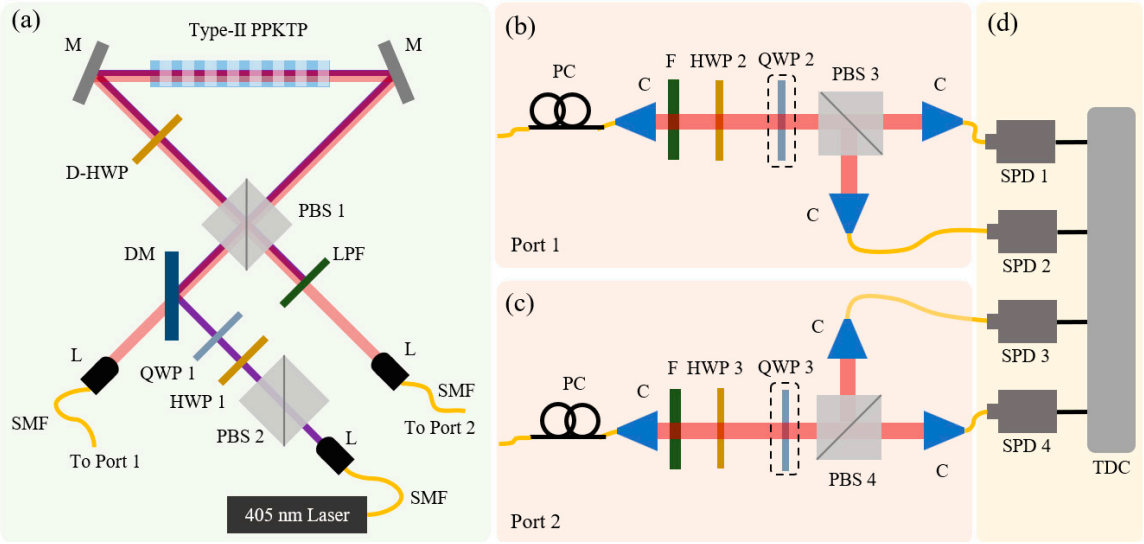

Figure 1. (**a**) Schematic of the airborne entangled-photon source (AEPS). (**b**,**c**) Experimental setup for the CHSH test and quantum state tomography (QST). When a QWP is inserted into the optical path, the setup can be used for QST. (**d**) Coincidence count part. SMF, single-model fiber; M, mirror; D-HWP, dual-wavelength half-wave plate; QWP, quarter-wave plate; PBS, polarization beam splitter; DM, dichroic mirror; LPF, long-pass filter; PC, polarization controller; L, lens; C, collimator; F, filter; SPD, single photon detector; and TDC, time-to-digital converter.

Figure 2 shows a photograph of the ultra-compact entangled-photon source. The entire module is only slightly larger than a coin, with dimensions of 38 × 40 × 24 mm^3 and a total weight of just 58 g, including the TEC, the silicon baseplate, and all optical elements. The integrated design not only offers significant advantages in size and weight but also enhances structural robustness, thereby improving the stability of quantum communication systems.

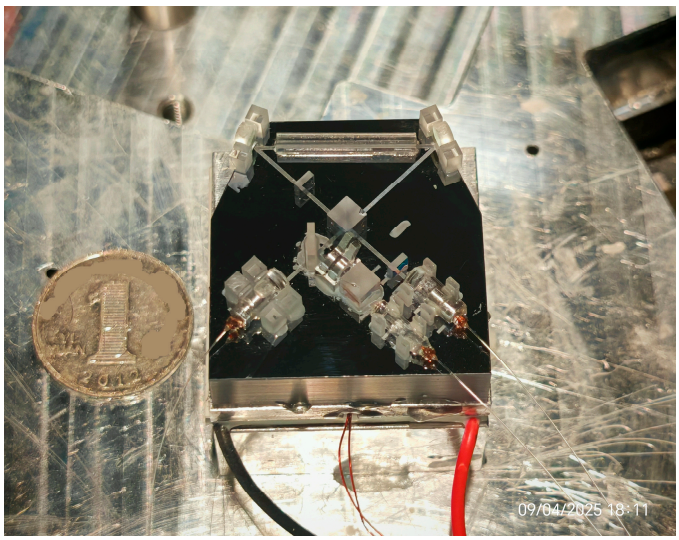

Figure 2. Photograph of the ultra-compact entangled-photon source module.

3. Results

This section presents the results of a series of performance characterizations of the entangled-photon source. We comprehensively examine the properties of the source from different perspectives, including measurements of the CHSH Bell inequality, entanglement visibility, quantum state tomography, and calculations of the generation rate and heralding efficiency.

3.1. CHSH-Type Bell Inequality

To determine whether the photon pairs exhibit non-local correlations, John Bell derived the famous Bell inequality. If experimental results violate this inequality, it demonstrates the existence of quantum entanglement and non-locality [32]. The CHSH inequality is a commonly used Bell inequality in experiments, proposed by Clauser, Horne, Shimony, and Holt in 1969 [33]. The inequality consists of four quantum correlation functions and is expressed as

$$S = E(a,b) - E(a,b') + E(a',b) + E(a',b'). \quad (1)$$

If $S \leq 2$, the photon pairs are classically correlated. If $S > 2$, the prepared state exhibits quantum non-locality, indicating it is an entangled state. When $S = 2\sqrt{2}$, the state is a maximally entangled Bell state, known as the Tsirelson bound [34].

The measurement process of the S value is as follows: First, the basis of one measurement setup was sequentially set to $|H\rangle$, $|V\rangle$, $|D\rangle$ and $|A\rangle$, corresponding to half-wave plate rotation angles of 0°, 45°, 22.5°, and 67.5° (Bell test angles). To achieve the maximum violation of the Bell inequality [35], the half-wave plate rotation angles for the other measurement setup were sequentially rotated to 11.25°, 56.25°, 33.75°, and 78.75°, completing 16 projection measurements of the state. The four single-photon detectors used in the experiment are Si-based APD (SPD500A-PC, LBTEK, Changsha Lubon Photoelectric Technology, Changsha, China), with a quantum efficiency of approximately 50% at 810 nm and dark counts less than 1 kHz. The TDC has a coincidence window of 3 ns, and the measurement time is 5 s. Table 2 shows one set of CHSH inequality test results for the entangled-photon source under a pump power of 0.37 mW. The coincidence counts, and the CHSH Bell parameter were measured repeatedly at different times within a day, yielding a set of closely similar S values. The average value of S was 2.764 with a standard deviation of 0.082, exceeding the classical bound of 2 by 9.3 standard deviations, demonstrating stability of the entangled-photon source.

Table 2. CHSH inequality measurement results.

	11.25°	56.25°	33.75°	78.75°
H	5905	32,160	31,778	5896
V	33,250	6754	5985	36,119
D	7293	36,017	6007	37,360
A	31,100	6105	32,100	5825

3.2. Two-Photon Correlation Curves

The two-photon correlation curve characterizes the interference contrast of entangled photons under different polarization bases. The testing procedure is similar to that of the CHSH test. One of the measurement setups was selected and set to the $|H\rangle$, $|V\rangle$, $|D\rangle$, and $|A\rangle$ bases by rotating the half-wave plate. The other measurement device was then scanned over all polarization states within the full 180° range, with coincidence counts recorded every 10°. As a result, four two-photon correlation curves were obtained

under the four bases, as shown in Figure 3. Each curve was fitted with a sine function, yielding adjusted R^2 values greater than 0.99, indicating an excellent fitting performance. By calculating the maximum (M) and minimum (m) coincidence counts of each correlation curve, the entanglement visibility for the corresponding basis was obtained, which is defined as follows:

$$V = \frac{M - m}{M + m}. \tag{2}$$

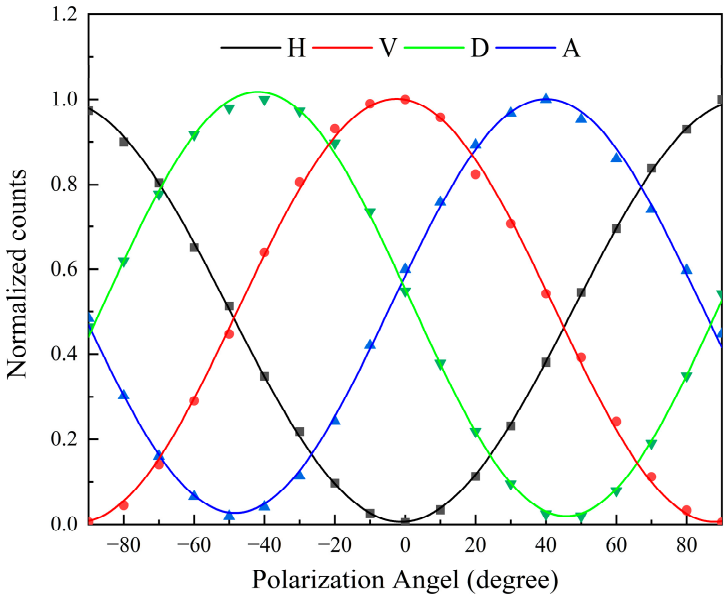

Figure 3. Two-photon correlation curves measured in the lab.

The test results show that the entangled-photon source achieves entanglement visibility of 98.6%, 98.7%, 96.7%, and 97.9% for the four measurement bases of $|H\rangle$, $|V\rangle$, $|D\rangle$, and $|A\rangle$, respectively.

3.3. Quantum State Tomography

Quantum state tomography provides a complete description of the quantum system's state and is a commonly used method for reconstructing the density matrix of a quantum system. This is achieved by projecting the quantum state onto different bases and performing measurements, followed by reconstructing the system's density matrix using maximum likelihood estimation. The density matrix can then be used to compute any physical quantities related to the quantum state [36]. By rotating the quarter-wave plates and half-wave plates in Port 1 and Port 2, the bases can be set to $|H\rangle$, $|V\rangle$, $|D\rangle$, and $|R\rangle$. The results of the 16 sets of coincidence counts are shown in Table 3.

Table 3. Quantum state tomography results.

	H	V	D	R
H	240	32,951	16,662	15,885
V	35,131	222	17,842	19,703
D	18,794	15,846	433	19,946
R	19,233	15,846	19,946	610

Fidelity is a crucial metric to quantify the similarity between the experimentally prepared state and the ideal target state, defined as [37]

$$F(\rho_1, \rho_2) = Tr\{\rho_1 \rho_2\}, \tag{3}$$

where ρ_1 denotes the reconstructed density matrix from experimental measurements, and ρ_2 represents the ideal target state. Using Equation (3), the fidelity of our system is calculated to be 0.986 ± 0.0017. The real and imaginary parts of the reconstructed density matrix are shown in Figure 4.

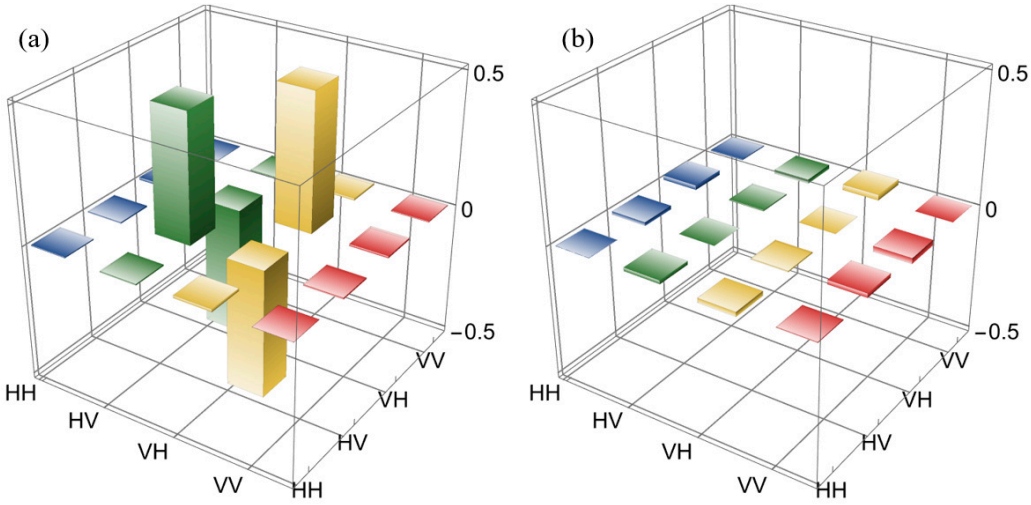

Figure 4. Reconstructed density matrix based on coincidence measurements: (**a**) real part and (**b**) imaginary part.

3.4. Generation Rate and Heralding Efficiency

The fidelity reflects the "quality" of the prepared entangled state, while the generation rate (γ) indicates the efficiency and brightness of the entangled-photon source, representing the number of entangled-photon pairs generated per second per unit pump power. In free-space QKD experiments, due to factors such as alignment errors in acquiring, pointing, and tracking (APT) systems, diffraction losses in the link, and the effects of atmospheric turbulence, the QKD link experiences significant losses. Therefore, it is crucial for the AEPS to achieve a high generation rate to overcome the high losses in the QKD link. Heralding efficiency ($\eta_{i,(s)}$), also known as the coincidence-to-singles ratio, characterizes the conditional probability that the idler (signal) will also be successfully detected when the signal (idler) is detected. The relationship between the generation rate and heralding efficiency for the entangled-photon source is given by the following equation [38]:

$$\gamma = \frac{R_s R_i}{R_c}, \tag{4}$$

$$\eta_{i,(s)} = \frac{R_c}{R_{s,(i)}}. \tag{5}$$

The R_s and R_i represent single-photon count rates of the signal and idler photons, respectively, while R_c represents the coincidence count rate measured by the TDC. Based on the measured coincidence counts, a generation rate of 1.12×10^6 pairs/s was inferred at a pump power of 0.37 mW, corresponding to a normalized generation rate of 3.03×10^6 pairs/s/mW for the entangled-photon source.

Numerous theoretical and experimental studies have shown that by adjusting the crystal length, the waist size of the pump beam in the crystal, and the parameters of the

coupling lenses, both heralding efficiency and generation rate can be improved [24,39–42]. However, as shown by Equation (5), the generation rate and heralding efficiency of the entangled-photon source cannot simultaneously achieve their maximum values, requiring a trade-off between the two. Based on the findings of Fedrizzi et al. [24], the chosen PPKTP crystal length for this experiment was 20 mm, with the 405 nm pump laser focused by a lens with a focal length of f = 2.8 mm to produce a 26 μm waist at the center of the crystal. The fiber coupler for the 810 nm entangled-photon pairs used a lens with a focal length of f = 3.2 mm. Experimental tests showed that the heralding efficiency for the signal photon was 13.67%, for the idler photon was 16.24%, and the symmetric heralding efficiency $\eta_{si} = R_c/\sqrt{R_s R_i}$ was 14.47%. In the study by Fedrizzi et al., for a 20 mm long PPKTP crystal operated at the optimized focal spot waist that maximizes the detected coincidence rate, the heralding efficiency is approximately 19%, which is close to the value observed in our experiment.

4. Discussion

By utilizing custom small-sized optical components and adhesive bonding techniques, we have achieved a compact and lightweight polarization-entangled photon source. Compared to traditional polarization-entangled sources, the entangled source we developed offers a 1–2 order of magnitude reduction in both volume and weight. The lightweight system and the thermally stable adhesive bonding contribute to the improved stability of our entangled source, making it more suitable for field-based quantum communication experiments in complex environments. At the same time, the performance characterization of the entangled source is comparable to that of traditional polarization-entangled sources.

On the other hand, there is still room for improvement in the heralding efficiency of our compact and lightweight entangled source. Existing literature has made both theoretical and experimental advances in increasing heralding efficiency. For instance, Palacios et al. [39], starting from the Heisenberg picture, derived the optimal relationship between the pump beam waist size, nonlinear crystal length, and wavevector. When the optimal focusing parameters for both pump and idler photons are chosen, the heralding efficiency can reach up to 78%. However, no practical Sagnac-type polarization-entangled source has yet achieved heralding efficiency close to the calculated result in this study. As discussed by Fedrizzi et al., achieving the highest detected coincidence-count rate requires a trade-off between brightness and heralding efficiency, as tight pump focusing enhances nonlinearity while exciting higher-order transverse modes that reduce fiber-coupling efficiency. In our source, the slightly lower heralding efficiency is mainly attributed to the use of Grin lenses instead of conventional aspheric lenses for single-mode fiber coupling, which was chosen to achieve a higher level of compactness. Nevertheless, the achieved brightness is sufficient for drone-based entanglement distribution, and future improvements will employ miniature aspheric lenses and narrower bandwidth filters to enhance the heralding efficiency.

5. Conclusions and Outlook

In this paper, we have developed a compact, lightweight, robust, and highly stable polarization-entangled photon source for use on mobile platforms such as drones. By employing small custom optical components, combined with adhesive bonding techniques, we have integrated the entire entangled-photon source onto a monocrystalline silicon substrate slightly larger than a coin, significantly enhancing the system's compactness and stability. The entire entangled source has a volume of only $38 \times 40 \times 24$ mm^3 and weighs just 58 g. Compared to previous Sagnac-type entangled sources, our source shows a 1–2 order of magnitude improvement in both volume and weight. The entangled source utilizes a 20 mm

long Type-II PPKTP crystal, pumped at 405 nm, to generate 810 nm entangled-photon pairs. The entanglement visibility is 98.6%, 98.7%, 96.7%, and 97.9% for the $|H\rangle$, $|V\rangle$, $|D\rangle$, and $|A\rangle$ bases, respectively. The CHSH inequality measurement yields $S = 2.764 \pm 0.082$, and the quantum state tomography test results show a fidelity of 0.986 ± 0.0017. The photon-pair generation rate at 810 nm is as high as 3.03×10^6 pairs/s/mW. The entire entangled-photon source is extremely compact, low-power, and highly stable, making it particularly suitable for mobile quantum communication experiments on low-load platforms like drones. The ultra-compact entangled source developed in this work will accelerate the advancement of mobile quantum internet construction.

In practical field testing, stable operation of entangled-photon sources is challenged by environmental temperature fluctuations, atmospheric turbulence, and platform-induced vibrations. To deal with the impact of temperature variations, the entangled-photon source was enclosed in a sealed, temperature-controlled housing. Together with the intrinsic temperature stabilization of the source itself, this dual-layer temperature-control design effectively isolates the entangled-photon source from ambient temperature fluctuations. Field testing indicates that the photon-pair generation rate measured inside the housing is consistent with that obtained under laboratory conditions. To address atmospheric disturbances and vibrations from the drone, a vibration-damping structure was designed between the housing of the source and the drone to reduce vibration effects.

The source developed in this work is fully single-mode fiber coupled with the 810 nm entangled-photon pairs delivered through single-mode fiber outputs. This design is compatible with APT systems, whose signal input ports are also based on single-mode fiber interfaces. Therefore, the entangled-photon source can be directly integrated with the APT system via fiber-to-fiber connection. The use of single-mode fibers ensures high spatial mode quality of the emitted photons, enabling efficient beam collimation in the optical transmitting module of the APT system. As a result, near-diffraction-limited beam divergence can be achieved in free-space transmission. In the future, this compact entangled-photon source can be used for applications including drone-based entanglement distribution, entanglement-based quantum key distribution, etc.

Author Contributions: Conceptualization, H.-Y.L. and Z.X.; methodology, J.W., X.-T.Z., H.-Y.L. and N.L.; software, J.W., N.L. and H.-Y.L.; validation, J.W., P.L., H.-Y.L., Z.X. and S.-N.Z.; formal analysis, J.W., P.L. and H.-Y.L.; investigation, J.W., P.L., X.-T.Z., H.-Y.L. and Z.X.; resources, P.W., L.S. and N.L.; data curation, J.W., P.L. and H.-Y.L.; writing—original draft preparation, J.W.; writing—review and editing, J.W., P.L., H.-Y.L., Y.-X.G. and Z.X.; visualization, J.W. and H.-Y.L.; supervision, H.-Y.L.; project administration, H.-Y.L.; funding acquisition, H.-Y.L. and Z.X. All authors have read and agreed to the published version of the manuscript.

Funding: This work was supported by the National Key R&D Program of China (2025YFF0524600), the National Natural Science Foundation of China (62293523, 62293520, 62550160), the Fundamental Research Funds for Central Universities (021014380250), and the Postgraduate Education Reform Project of Jiangsu Province (2025JGZD090).

Institutional Review Board Statement: Not applicable.

Informed Consent Statement: Not applicable.

Data Availability Statement: The original contributions presented in this study are included in the article. Further inquiries can be directed to the corresponding author(s).

Conflicts of Interest: The authors declare no conflicts of interest.

Abbreviations

The following abbreviations are used in this manuscript:

QKD	Quantum key distribution
AEPS	Airborne entangled-photon source
SPDC	Spontaneous parametric down-conversion
PPKTP	Periodically poled $KTiOPO_4$
FWM	Four-wave mixing
SiC	Silicon carbide
Si-APD	Silicon avalanche photodiodes
SNSPD	Superconducting-nanowire single-photon detectors
QPM	Quasi-phase matching
APT	Acquiring, pointing, and tracking

References

1. Tian, X.-H.; Yang, R.; Liu, H.-Y.; Fan, P.; Zhang, J.-N.; Gu, C.; Chen, M.; Hu, M.; Lu, F.-Y.; Zhu, C.; et al. Experimental Demonstration of Drone-Based Quantum Key Distribution. *Phys. Rev. Lett.* **2024**, *133*, 200801. [CrossRef]
2. Liu, H.-Y.; Tian, X.-H.; Gu, C.; Fan, P.; Ni, X.; Yang, R.; Zhang, J.-N.; Hu, M.; Guo, J.; Cao, X.; et al. Drone-Based Entanglement Distribution towards Mobile Quantum Networks. *Natl. Sci. Rev.* **2020**, *7*, 921–928. [CrossRef]
3. Liu, H.-Y.; Tian, X.-H.; Gu, C.; Fan, P.; Ni, X.; Yang, R.; Zhang, J.-N.; Hu, M.; Guo, J.; Cao, X.; et al. Optical-Relayed Entanglement Distribution Using Drones as Mobile Nodes. *Phys. Rev. Lett.* **2021**, *126*, 020503. [CrossRef]
4. Li, Y.; Cai, W.-Q.; Ren, J.-G.; Wang, C.-Z.; Yang, M.; Zhang, L.; Wu, H.-Y.; Chang, L.; Wu, J.-C.; Jin, B.; et al. Microsatellite-Based Real-Time Quantum Key Distribution. *Nature* **2025**, *640*, 47–54. [CrossRef]
5. Zhong, H.-S.; Wang, H.; Deng, Y.-H.; Chen, M.-C.; Peng, L.-C.; Luo, Y.-H.; Qin, J.; Wu, D.; Ding, X.; Hu, Y.; et al. Quantum Computational Advantage Using Photons. *Science* **2020**, *370*, 1460–1463. [CrossRef]
6. Deng, Y.-H.; Gu, Y.-C.; Liu, H.-L.; Gong, S.-Q.; Su, H.; Zhang, Z.-J.; Tang, H.-Y.; Jia, M.-H.; Xu, J.-M.; Chen, M.-C.; et al. Gaussian Boson Sampling with Pseudo-Photon-Number-Resolving Detectors and Quantum Computational Advantage. *Phys. Rev. Lett.* **2023**, *131*, 150601. [CrossRef] [PubMed]
7. Liu, L.-Z.; Zhang, Y.-Z.; Li, Z.-D.; Zhang, R.; Yin, X.-F.; Fei, Y.-Y.; Li, L.; Liu, N.-L.; Xu, F.; Chen, Y.-A.; et al. Distributed Quantum Phase Estimation with Entangled Photons. *Nat. Photonics* **2021**, *15*, 137–142. [CrossRef]
8. Hong, S.; ur Rehman, J.; Kim, Y.-S.; Cho, Y.-W.; Lee, S.-W.; Jung, H.; Moon, S.; Han, S.-W.; Lim, H.-T. Quantum Enhanced Multiple-Phase Estimation with Multi-Mode N00N States. *Nat. Commun.* **2021**, *12*, 5211. [CrossRef]
9. Samad, M.; Shimizu, M.; Hijikata, Y. Demonstration of Quantum Polarized Microscopy Using an Entangled-Photon Source. *Photonics* **2025**, *12*, 127. [CrossRef]
10. Bie, S.; Tong, X.; Lv, Z.; Ye, H.; Cao, T. Using Cyclic Hadamard Masks for Single-Pixel Quantum Imaging under Entangled Photon Illumination. *Sci. Adv.* **2025**, *11*, eadw4799. [CrossRef]
11. Yin, J.; Cao, Y.; Li, Y.-H.; Liao, S.-K.; Zhang, L.; Ren, J.-G.; Cai, W.-Q.; Liu, W.-Y.; Li, B.; Dai, H.; et al. Satellite-Based Entanglement Distribution over 1200 Kilometers. *Science* **2017**, *356*, 1140–1144. [CrossRef] [PubMed]
12. Liao, S.-K.; Cai, W.-Q.; Liu, W.-Y.; Zhang, L.; Li, Y.; Ren, J.-G.; Yin, J.; Shen, Q.; Cao, Y.; Li, Z.-P.; et al. Satellite-to-Ground Quantum Key Distribution. *Nature* **2017**, *549*, 43–47. [CrossRef]
13. Conrad, A.; Isaac, S.; Cochran, R.; Sanchez-Rosales, D.; Rezaei, T.; Javid, T.; Schroeder, A.; Golba, G.; Gauthier, D.; Kwiat, P.G. Drone-Based Quantum Communication Links. In *Quantum Computing, Communication, and Simulation III*; Hemmer, P.R., Migdall, A.L., Eds.; SPIE: San Francisco, CA, USA, 2023; p. 42.
14. Conrad, A.; Cochran, R.; Sanchez-Rosales, D.; Isaac, S.; Javid, T.; Rezaei, T.; Schroeder, A.J.; Golba, G.; Gutha, A.; Wilens, B.; et al. Drone- and Vehicle-Based Quantum Key Distribution. *arXiv* **2025**, arXiv:2505.17587. [CrossRef]
15. Conrad, A.; Isaac, S.; Cochran, R.; Sanchez-Rosales, D.; Javid, T.; Gauthier, D.J.; Kwiat, P.G. Vehicle-to-Vehicle Quantum Key Distribution (V2V-QKD). In *Proceedings of the CLEO 2024, Charlotte, NC, USA, 5–10 May 2024*; Optica Publishing Group: Charlotte, NC, USA, 2024; p. AW4D.4.
16. Omshankar; Venkataraman, V.; Ghosh, J. Bright Source of Narrowband Polarization-Entangled Photons from a Thick Type-II ppKTP Crystal. *Opt. Express* **2024**, *32*, 3470. [CrossRef] [PubMed]
17. Jin, H.; Liu, F.M.; Xu, P.; Xia, J.L.; Zhong, M.L.; Yuan, Y.; Zhou, J.W.; Gong, Y.X.; Wang, W.; Zhu, S.N. On-Chip Generation and Manipulation of Entangled Photons Based on Reconfigurable Lithium-Niobate Waveguide Circuits. *Phys. Rev. Lett.* **2014**, *113*, 103601. [CrossRef]

18. Xue, G.-T.; Niu, Y.-F.; Liu, X.; Duan, J.-C.; Chen, W.; Pan, Y.; Jia, K.; Wang, X.; Liu, H.-Y.; Zhang, Y.; et al. Ultrabright Multiplexed Energy-Time-Entangled Photon Generation from Lithium Niobate on Insulator Chip. *Phys. Rev. Appl.* **2021**, *15*, 064059. [CrossRef]
19. Horn, R.; Abolghasem, P.; Bijlani, B.J.; Kang, D.; Helmy, A.S.; Weihs, G. Monolithic Source of Photon Pairs. *Phys. Rev. Lett.* **2012**, *108*, 153605. [CrossRef]
20. Guo, X.; Zou, C.; Schuck, C.; Jung, H.; Cheng, R.; Tang, H.X. Parametric Down-Conversion Photon-Pair Source on a Nanophotonic Chip. *Light Sci. Appl.* **2017**, *6*, e16249. [CrossRef]
21. Rahmouni, A.; Wang, R.; Li, J.; Tang, X.; Gerrits, T.; Slattery, O.; Li, Q.; Ma, L. Entangled Photon Pair Generation in an Integrated SiC Platform. *Light Sci. Appl.* **2024**, *13*, 110. [CrossRef]
22. Ou, H. Silicon Carbide, the next-Generation Integrated Platform for Quantum Technology. *Light Sci. Appl.* **2024**, *13*, 219. [CrossRef]
23. Chen, X.; Fu, Z.; Gong, Q.; Wang, J. Quantum Entanglement on Photonic Chips: A Review. *Adv. Photonics* **2021**, *3*, 064002. [CrossRef]
24. Fedrizzi, A.; Herbst, T.; Poppe, A.; Jennewein, T.; Zeilinger, A. A Wavelength-Tunable Fiber-Coupled Source of Narrowband Entangled Photons. *Opt. Express* **2007**, *15*, 15377. [CrossRef] [PubMed]
25. Feng, L.-T.; Zhang, M.; Zhou, Z.-Y.; Chen, Y.; Li, M.; Dai, D.-X.; Ren, H.-L.; Guo, G.-P.; Guo, G.-C.; Tame, M.; et al. Generation of a Frequency-Degenerate Four-Photon Entangled State Using a Silicon Nanowire. *npj Quantum Inf.* **2019**, *5*, 90. [CrossRef]
26. Liu, J.; Su, R.; Wei, Y.; Yao, B.; da Silva, S.F.C.; Yu, Y.; Iles-Smith, J.; Srinivasan, K.; Rastelli, A.; Li, J.; et al. A Solid-State Source of Strongly Entangled Photon Pairs with High Brightness and Indistinguishability. *Nat. Nanotechnol.* **2019**, *14*, 586–593. [CrossRef]
27. Ma, J.; Fan, T.; Haggren, T.; Molina, L.V.; Parry, M.; Shinde, S.; McManus-Barrett, C.; Zhang, J.; Morales, R.C.; Setzpfandt, F.; et al. Nonlinearity Symmetry Breaking for Generating Tunable Quantum Entanglement in Semiconductor Metasurfaces. *Sci. Adv.* **2025**, *11*, eadu4133. [CrossRef] [PubMed]
28. Jia, W.; Saerens, G.; Talts, Ü.-L.; Weigand, H.; Chapman, R.J.; Li, L.; Grange, R.; Yang, Y. Polarization-Entangled Bell State Generation from an Epsilon-near-Zero Metasurface. *Sci. Adv.* **2025**, *11*, eads3576. [CrossRef]
29. Armstrong, J.A. Interactions between Light Waves in a Nonlinear Dielectric. *Phys. Rev.* **1962**, *127*, 1918–1939. [CrossRef]
30. Anwar, A.; Perumangatt, C.; Steinlechner, F.; Jennewein, T.; Ling, A. Entangled Photon-Pair Sources Based on Three-Wave Mixing in Bulk Crystals. *Rev. Sci. Instrum.* **2021**, *92*, 041101. [CrossRef]
31. Beckert, E.; de Vries, O.; Ursin, R.; Steinlechner, F.-O.; Gräfe, M.; Basset, M.G. A Space-Suitable, High Brilliant Entangled Photon Source for Satellite Based Quantum Key Distribution. In *Free-Space Laser Communications XXXI*; SPIE: Bellingham, WA, USA, 2019; Volume 10910, pp. 260–273.
32. Bell, J.S. On the Einstein Podolsky Rosen Paradox. *Phys. Phys. Fiz.* **1964**, *1*, 195–200. [CrossRef]
33. Clauser, J.F.; Horne, M.A.; Shimony, A.; Holt, R.A. Proposed Experiment to Test Local Hidden-Variable Theories. *Phys. Rev. Lett.* **1969**, *23*, 880–884. [CrossRef]
34. Cirel'son, B.S. Quantum Generalizations of Bell's Inequality. *Lett. Math. Phys.* **1980**, *4*, 93–100. [CrossRef]
35. Jöns, K.D.; Schweickert, L.; Versteegh, M.A.M.; Dalacu, D.; Poole, P.J.; Gulinatti, A.; Giudice, A.; Zwiller, V.; Reimer, M.E. Bright Nanoscale Source of Deterministic Entangled Photon Pairs Violating Bell's Inequality. *Sci. Rep.* **2017**, *7*, 1700. [CrossRef]
36. James, D.F.V.; Kwiat, P.G.; Munro, W.J.; White, A.G. Measurement of Qubits. *Phys. Rev. A* **2001**, *64*, 052312. [CrossRef]
37. Jozsa, R. Fidelity for Mixed Quantum States. *J. Mod. Opt.* **1994**, *41*, 2315–2323. [CrossRef]
38. Steinlechner, F.; Gilaberte, M.; Jofre, M.; Scheidl, T.; Torres, J.P.; Pruneri, V.; Ursin, R. Efficient Heralding of Polarization-Entangled Photons from Type-0 and Type-II Spontaneous Parametric Downconversion in Periodically Poled $KTiOPO_4$. *J. Opt. Soc. Am. B* **2014**, *31*, 2068–2076. [CrossRef]
39. Palacios, S.; de J. León-Montiel, R.; Hendrych, M.; Valencia, A.; Torres, J.P. Flux Enhancement of Photons Entangled in Orbital Angular Momentum. *Opt. Express* **2011**, *19*, 14108–14120. [CrossRef] [PubMed]
40. Ljunggren, D.; Tengner, M. Optimal Focusing for Maximal Collection of Entangled Narrow-Band Photon Pairs into Single-Mode Fibers. *Phys. Rev. A* **2005**, *72*, 062301. [CrossRef]
41. Guerreiro, T.; Martin, A.; Sanguinetti, B.; Bruno, N.; Zbinden, H.; Thew, R.T. High Efficiency Coupling of Photon Pairs in Practice. *Opt. Express* **2013**, *21*, 27641–27651. [CrossRef]
42. Bennink, R.S. Optimal Collinear Gaussian Beams for Spontaneous Parametric Down-Conversion. *Phys. Rev. A* **2010**, *81*, 053805. [CrossRef]

Disclaimer/Publisher's Note: The statements, opinions and data contained in all publications are solely those of the individual author(s) and contributor(s) and not of MDPI and/or the editor(s). MDPI and/or the editor(s) disclaim responsibility for any injury to people or property resulting from any ideas, methods, instructions or products referred to in the content.